Tenth International Conference on Computational Fluid Dynamics (ICCFD10), Barcelona, Spain, July 9-13, 2018

ICCFD10-166

Conceptual Design of Reusable Unmanned Space Vehicle Using MDO with MOGA

J. Jung*, K. You**, K. Park**, K. Yee* and S. Jeong**
Corresponding author: icarus@khu.ac.kr

* Seoul National University, Korea
** Kyunghee University, Korea.

Abstract: In this study, a conceptual design of a reusable unmanned space vehicle with multi-objective functions is conducted. To do that, the multi-objective genetic algorithm (MOGA) was used. To evaluate the performance of the space vehicles, several discipline were analyzed; weight, propulsion, aerothermodynamic and trajectory analysis. Three objective functions were selected; 1) minimization of weight, 2) minimization of landing speed and 3) maximization of the highest C_L in the supersonic range. Moreover, the maximum dynamic pressure and heat flux were considered as constraints. All objective functions are in trade-off relationships with each other. The smallest weight vehicle has a very small wing size. The vehicle which has the highest CL in supersonic range has a closer angle between the flow and the lower surface of wing to angle which shows the highest CL on the flat surface. The vehicle which has the lowest landing speed had the largest wing, which generate sufficient lift.

Keywords: Reusable Unmanned Space Vehicle, Conceptual Design, MDO, MOGA.

1 Introduction

To promote the development of space science, many scientific experiments has been performed. However, it is difficult that conditions for cosmic environment are simulated on the ground such as micro gravity. Therefore, various experiments has been conducted in space directly. If each experiments are executed with an expendable vehicle, it will be necessary to build the new vehicle every time, which is a huge expense. To reduce these costs, it is a need for reusable manned or unmanned space vehicles.

Reusable unmanned space vehicles are complex systems that have to be designed considering various disciplinary; aerothermodynamics, structure, weight, propulsion, trajectory, control, cost and so on. Therefore, a method for treating these disciplinary is necessary. Multidisciplinary optimization (MDO) is used widely for handling various disciplinary because MDO assembles various disciplinary and optimization, and identifies a feasible result quickly in the design space [1].

Several paper presents designing space vehicles with MDO. Lawrence designed a rocket-based single-stage-to-orbit vehicle based on weight, sizing, operations and cost analysis [2]. Tsuchiya designed a two-stage reusable rocket vehicle and a hypersonic experimental vehicle to reduce the weight through weight analysis, aerodynamic analysis, propulsion analysis, and trajectory analysis [3, 4]. Yokoyama designed a single-stage-to-orbit space plane by using weight, aerodynamic, and propulsion analysis [5]. Weight reduction is only the objective function in almost studies. However, reusable unmanned space vehicles should be considered on not only weight but also various objective

functions such as lift and landing speed because the vehicles are built for various purpose.

Therefore, the purpose of this study is to design a reusable unmanned space vehicle with multi objective functions. To do that, the current MDO is composed of vehicle geometry definition, weight analysis, propulsion analysis, aerothermodynamic analysis, trajectory analysis, and a multi-objective genetic algorithm (MOGA) [6]. To compare the geometry and performance, the extreme solutions were selected in a Pareto solution.

2 Analysis Method

The overall analysis and optimization process are shown in Fig. 1. As shown in the figure, each disciplinary effects on others and received an effect. Therefore, it is necessary to converge coupling variables through iterative calculations. After coupling variables are converged, the performance of each vehicle was calculated, and optimization was performed.

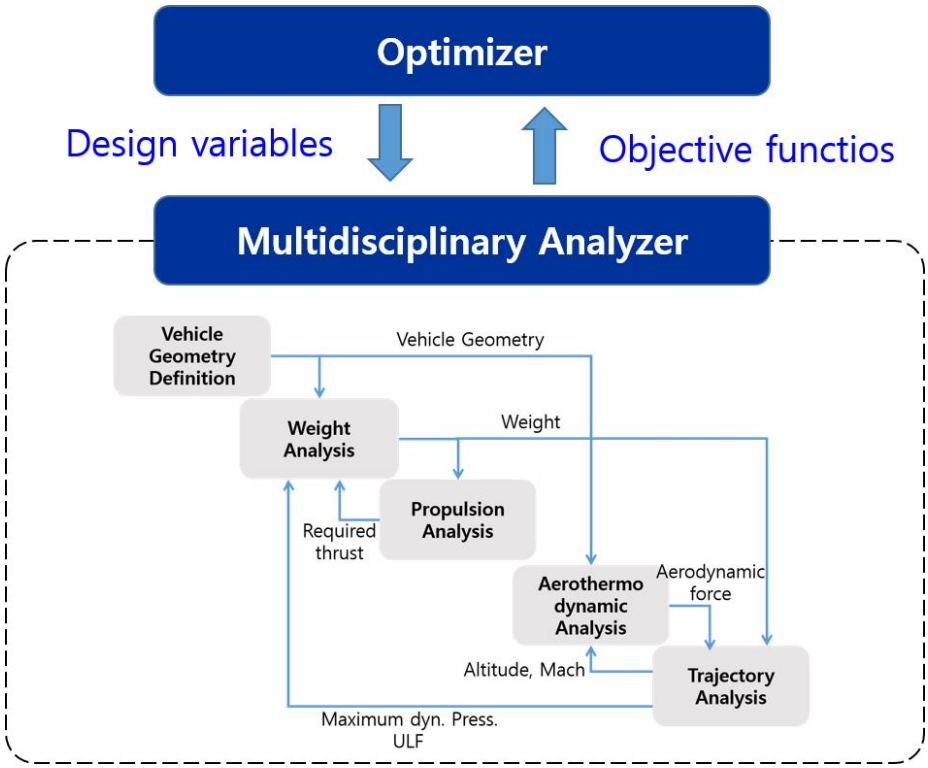

Figure 1: Overall MDO process.

2.1 Vehicle Geometry Definition

The fuselage is divided in three sections. One is nose section, and the others are two body section. The nose section is a part of sphere. The body sections are made up of one cross section, and the cross sections are defined by three variables; rectangular height, corner radius and width. To define the blunt node, spherically blunted tangent ogive curves were employed. The planform of the wings were defined by using for variables; sweep angle, span, tip chord and root chord. The airfoils of wings were defined as the NACA 4 digit. Moreover, two variables determined the location each wings. Figure 2 shows the variables used for defining the geometry, Table 1 summarizes a detail list of variables.

In addition, a rear body flap are considered. The width of the flap is the same as that of body section 2, and the length is 1/8 of the total length of the fuselage.

Table 1: Geometry variables.

Position	Variable description	Variable
Fuselage	Nose radius	dv 1
	Section 1 width	dv 2
	Section 1 rectangular height	dv 3
	Section 1 corner radius	dv 4
	Length of Section 1	dv 5
	Section 2 width	dv 6
	Section 2 rectangular height	dv 7
	Section 2 corner radius	dv 8
	Length of Section 2	dv 9
	Total length	dv 10
	Nose length	dv 11
	Nose height	dv 12
Main wing	Root chord	dv 13
	Tip chord	dv 14
	Leading edge sweep angle	dv 15
	Span	dv 16
	Incidence angle	dv 17
	Longitudinal location	dv 18
	Vertical location	dv 19
	Maximum camber	dv 10
	Camber location	dv 21
	Maximum thickness	dv 22
Horizontal wing	Root chord	dv 23
	Tip chord	dv 24
	Span	dv 25
	Incidence angle	dv 26
	Longitudinal location	dv 27
	Vertical location	dv 28
	Maximum camber	dv 29
	Camber location	dv 30
	Maximum thickness	dv 31
Vertical wing	Root chord	dv 32
	Tip chord	dv 33
	Leading edge sweep angle	dv 34
	Span	dv 35
	Longitudinal location	dv 36
	Maximum thickness	dv 37

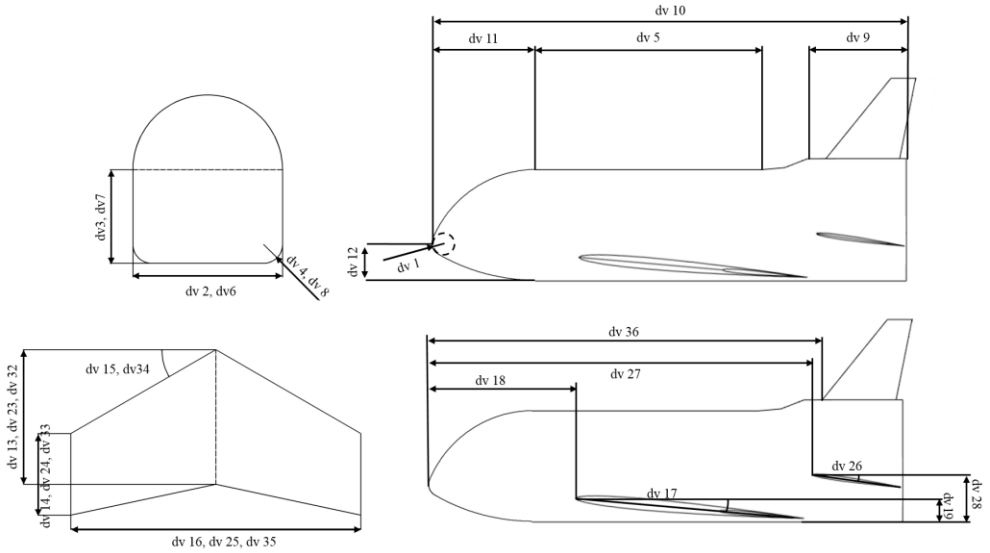

Figure 2: Geometry variables.

2.2 Weight Analysis

Weight analysis calculated the weight of the vehicle and the center of gravity. To calculate each part of the vehicle, Hypersonic Aerospace Sizing Analysis (HASA) was used in this study [7]. HASA estimates the weight by using statistical methods. However, to improve the accuracy, HASA was modified. That is because the statistical equations were formulated by using data from 100 t class vehicles, while the target of this study is about 2-3 t.

In this study, the vehicles enter mission orbit by launch vehicle. Since the fuel is used during the mission, the gross weight is heavier than the landing weight. Thus, weight of the landing gear should be estimated based on landing weight as follows [8],

$$W_{gear} = 0.03\, W_{land},$$

where W_{gear} is the weight of landing gear and W_{land} is the maximum landing weight.

The actual weight of the thermal protection system (TPS) was calculated form a product of the TPS density and the area. The type of TPS no surface was determined by referring to the Space Shuttle. On the nose and leading edge, a reinforced carbon-carbon (RCC) was applied. On the lower surface of the fuselage and the wing, high-temperature reusable surface insulation (HRSI) was applied. On the other parts, fibrous refractory composite insulation (FRSI) was applied. Figure 3 shows the type of TPS.

The weight of avionics was reduced from HASA using a reduction factor since technological development [9]. The weight of payload was assumed to be 226.8kg and the density was 52.86kg/m^3.

The estimated weight using modified HASA was compared with the actual weight of the Boeing X-37 [10]. However, because X-37 is for long-term missions, the Boeing X-37 has more fuel than the designed vehicles. Thus, to compare the estimated and actual weight, the fuel quantity was set to the actual fuel weight of the X-37. Table 2 summarizes the results of comparison. The error is very large (90.3%) when the original HASA. On the other hand, the estimated weight from the modified HASA is very similar with the actual weight within only 4.0% error.

2.3 Propulsion Analysis

In this study, because the space vehicles are entered into mission orbit, a main engine is not installed in the vehicles. However, to modify the orbit or the attitude, an orbital maneuvering system and a reaction control system (OMS / RCS) are necessary. The required thrusts of OMS /RCS were calculated to referring a paper in the literature [8]. The weight of the OMS/ RCS were calculated based on the required thrust. The thrust-to-weight ratio of the OMS, primary RCS and vernier RCS were 22, 39.5 and 9.4, respectively [8]. The values for the primary RCS and Vernier RCS were set to

Table 2: Actual weight of the Boeing X-37 and estimated weight.

	Actual weight	Original HASA (Error)	Modified HASA (Error)
Fuselage weight (kg)		776.6	468.4
Wing weight (kg)		270.8	139.7
Tail wing weight (kg)		183.9	95.0
TPS weight (kg)		122.6	454.8
Landing gear weight (kg)		243.9	99.0
Tank weight (kg)		66.51	187.5
Engine weight (kg)		62.13	808.5
Misc. weight (kg)		5974.3	741.5
Dry weight (kg)		7927.5	3221.2
LH2 weight (kg)		224.9	224.9
LOX weight (kg)		1342.6	1342.6
Gross Weight (kg)	4,990	9495 (90.3%)	4789 (4.0%)

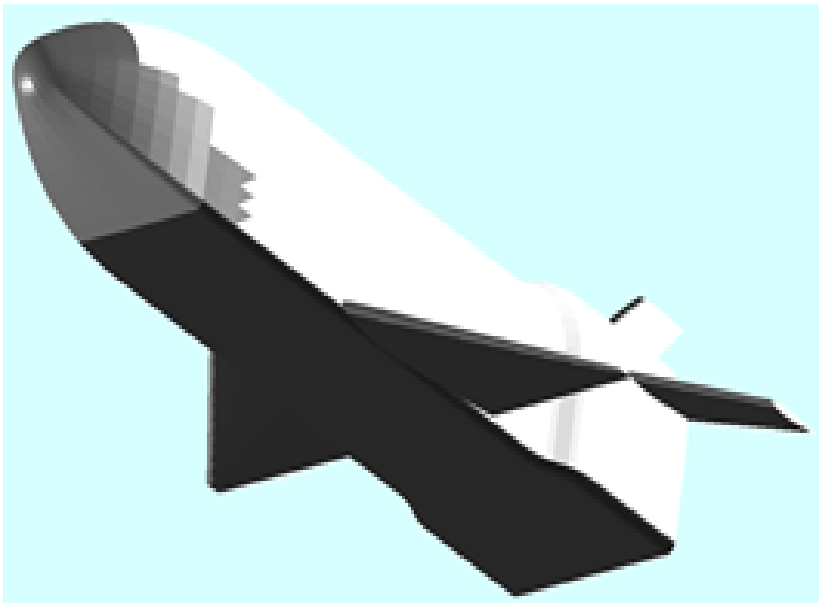

Figure 3: Type of TPS on each surface.

38 and 6, respectively, by referring to the Space Shuttle.

A cryogenic propellant fuel (LOX / LH2) were used for the OMS/ RCS. The total fuel weight was calculated based on the required thrust [8]. Each tank of fuel was composed of a cylinder with dome-shape ends. The radius of the tank was the same as that of the circle tangent to the body section, as shown in Fig. 4.

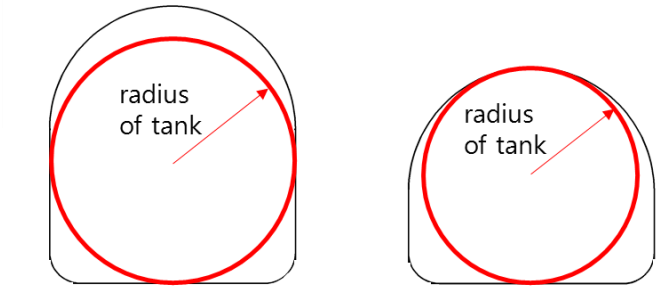

Figure 4: Radius of fuel tank.

2.4 Aerothermodynamic Analysis

The space vehicles passes a wide speed range from hypersonic to subsonic. The aerodynamic properties were calculated by using modified Newtonian impact theory in hypersonic and supersonic range. And by Digital DATCOM in subsonic range [11, 12]. Furthermore, aerodynamic analysis evaluated the longitudinal stability. To maintain longitudinal stability, this is one of the constraints. To determine whether or not the longitudinal stability can be maintained, the center of gravity calculated from the weight analysis and pressure distribution were used. The angle of attack, which is used to evaluate the aerodynamic force, varies with the Mach number. The angle of attack along the Mach number is shown in Fig. 5 [13].

The amount of heat flux by aerodynamic heating have to be evaluated because the vehicle passes through hypersonic and supersonic. The formula for calculating the heat flux is expressed as follows [14].

$$\dot{q} = 9.4369 \times 10^{-5} \sqrt{\rho}\, V^{3.15}$$

To prevent excessive heat flux and load on the vehicles, the heat flux and dynamic pressure were limited to 4MW/m^2 and 50kPa, respectively.

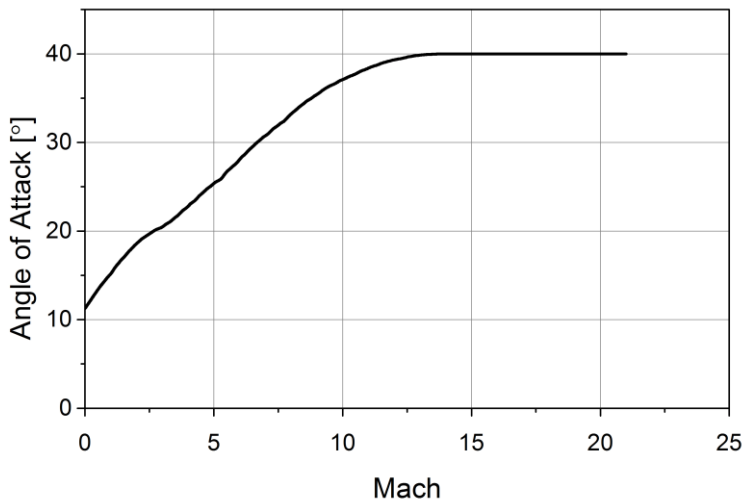

Figure 5: Pre-described angle of attack to the Mach number.

2.5 Trajectory Analysis

Three degree of freedom (3DOF) trajectory analysis was employed. In this study, since the vehicles enter orbit using the launch vehicle, the trajectory of the vehicles was evaluated only from the orbit to the landing. Table 3 summarizes the initial conditions of trajectory. For time marching, the 4th Runge Kutta method was used.

Table 3: Initial trajectory condition.

Initial trajectory condition	Value
Altitude	300km
Velocity	7000m/s
Flight path angle	0˚
Incline angle	80˚

3 Optimization

3.1 Optimization Algorithm

In this study, a real-coded MOGA was adopted for the MDO to account for the multiple objective functions. Figure 6 shows the overall procedure for the optimization process. It is well known that GAs require a large computational cost due to population-based searches. Therefore, the evaluation of each individual was run in parallel. Figure 7 shows a schematic of a parallelized evaluation of each individual.

3.2 Definition of the Optimization Problem

In MOGA, the population and generation numbers were set to 256 and 100, respectively. There are three objective functions as follows;

1) Minimize weight
2) Maximize the highest CL in the supersonic range where Mach number is larger than unity
3) Minimize landing speed.

As constraints, maximum heat flux and maximum dynamic pressure must be below 4MW/m2 and 50kPa, respectively, and the longitudinal stability should be maintained.

4 Result

Figure 8 shows the Pareto solutions plotted in objective function space. All the objective functions are in trade-off relationships with each other. To identify geometry features, extreme solutions and compromised solution from Pareto solution were selected. The lightest vehicle in the Pareto solution is named ‘OPT1’. The vehicle with the highest maximum C_L in the supersonic range in the Pareto solution is named ‘OPT2’. The vehicle with the slowest landing speed in the Pareto solution is named

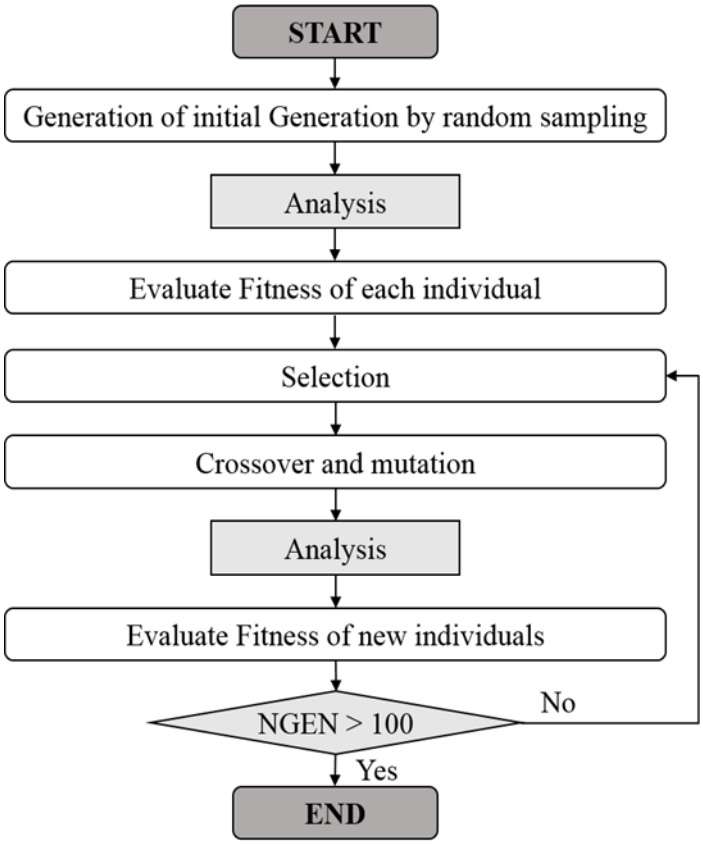

Figure 6: Flowchart for the optimization precess.

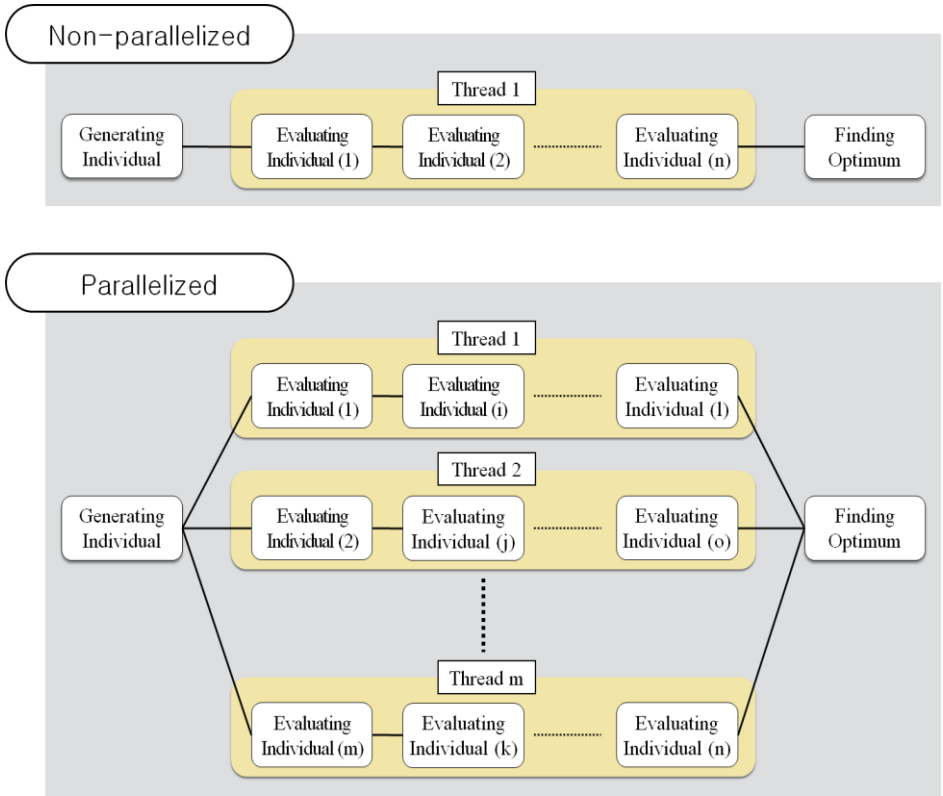

Figure 7: Summary of parallel evaluation of the objective function.

'OPT3', and the vehicle which is a compromise solution with regard to all objective functions is named 'OPT4'. Figure 9 shows the geometries of OPT1-4, and Table 4 summarizes the performance and weight data of OPT1-4.

The width of the fuselage of OPT1-4 is larger than the height of that in Fig. 9. Thus, C_L is increased by widening the area directly receiving the flow.

The wing of OPT1 is the smallest. From this, the overall weight was reduced by cutting the weight of the wings.

When the angle between the flow and flat surface is 54.74° in modified Newtonian theory, C_L is maximum. The angle between the flow and the lower surface of wing of OPT2 in the wider range is closer to 54.74° than that of the others, as shown in Fig. 10. Therefore, the wing of OPT2 can generate more lift coefficient than that of the others, such as those in Fig. 11.

The altitude and velocity of OPT3 deceased earlier than the others, as shown in Fig. 12. This is why the largest wing of OPT3 causes more drag. However, a lot of lift was generated from the largest wing, and sufficient deceleration was achieved during the fall, resulting in a lower landing speed.

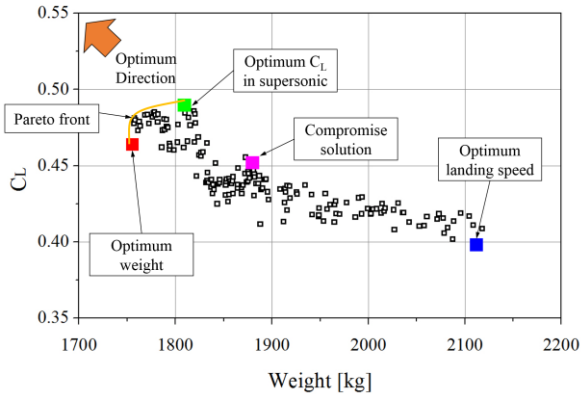

(a) Weight and C_L

Figure 8: Pareto solution of each pair of objective functions.

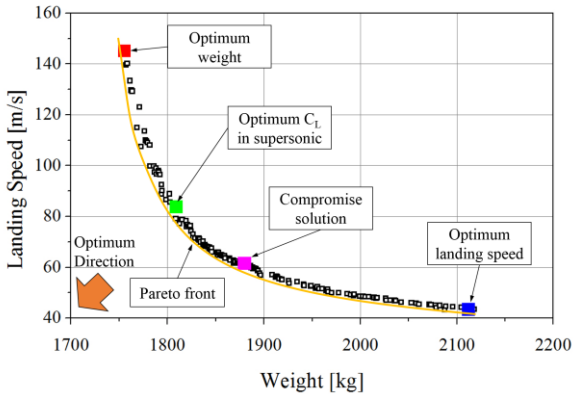

(b) Weight and landing speed

Figure 8: Pareto solution of each pair of objective functions.

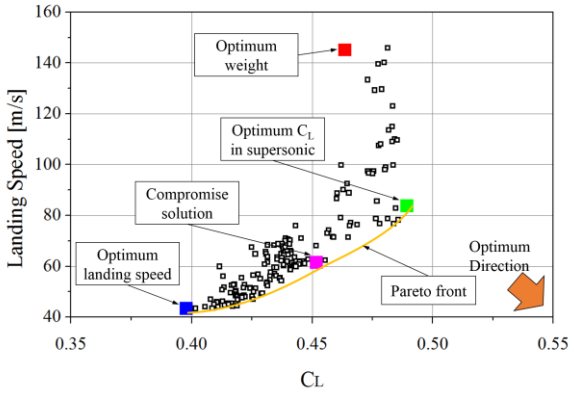

(b) C_L and landing speed

Figure 8: Pareto solution of each pair of objective functions.

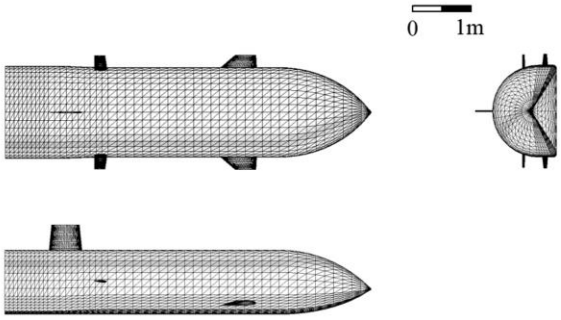

(a) OPT1

Figure 9: Geometries of OPT1-4.

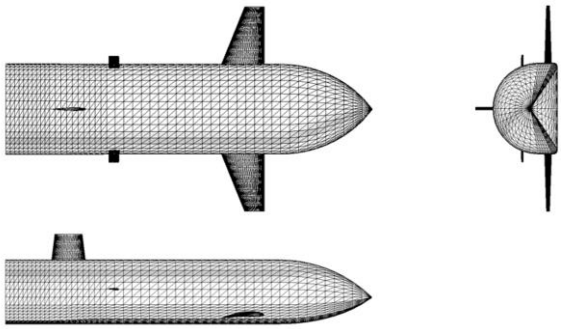

(b) OPT2

Figure 9: Geometries of OPT1-4.

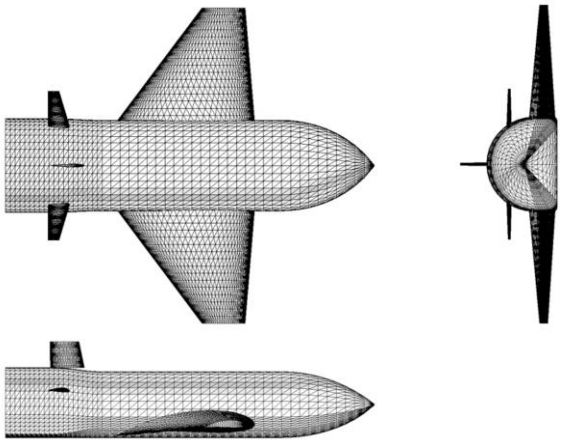

(c) OPT3

Figure 9: Geometries of OPT1-4.

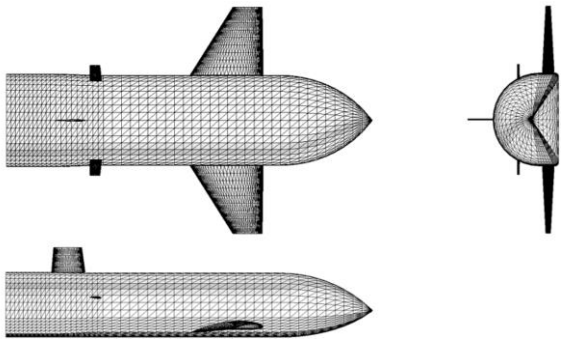

(d) OPT4

Figure 9: Geometries of OPT1-4.

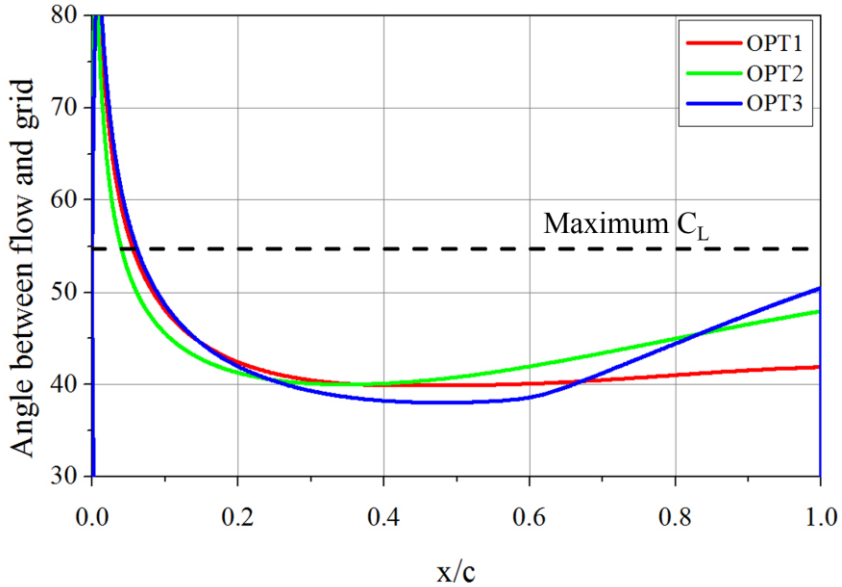

Figure 10: Distribution of angle between the flow and the lower surface on the mid-span of wing of OPT1-3 at Mach number = 20 and angle of attack = 40˚.

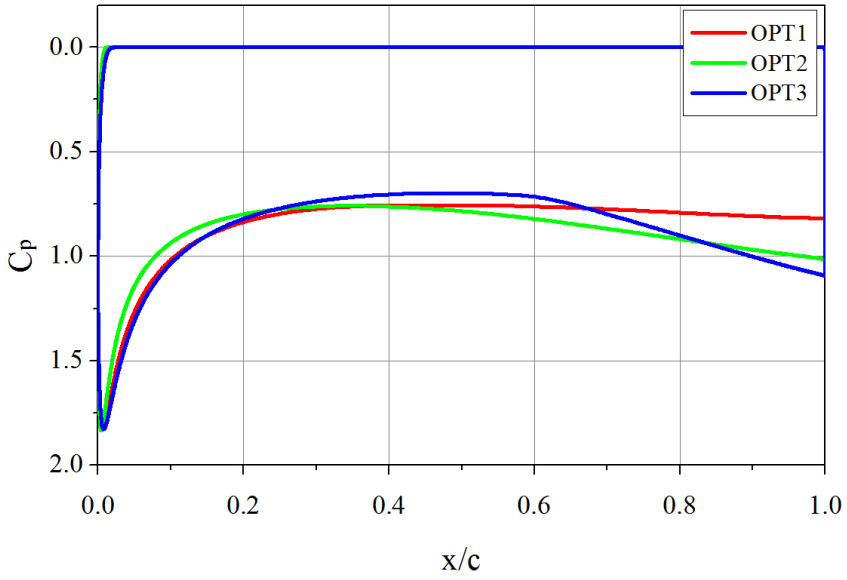

Figure 11: C_p distribution on mid-span of wing of OPT1-3 at Mach number = 20 and angle of attack = 40˚.

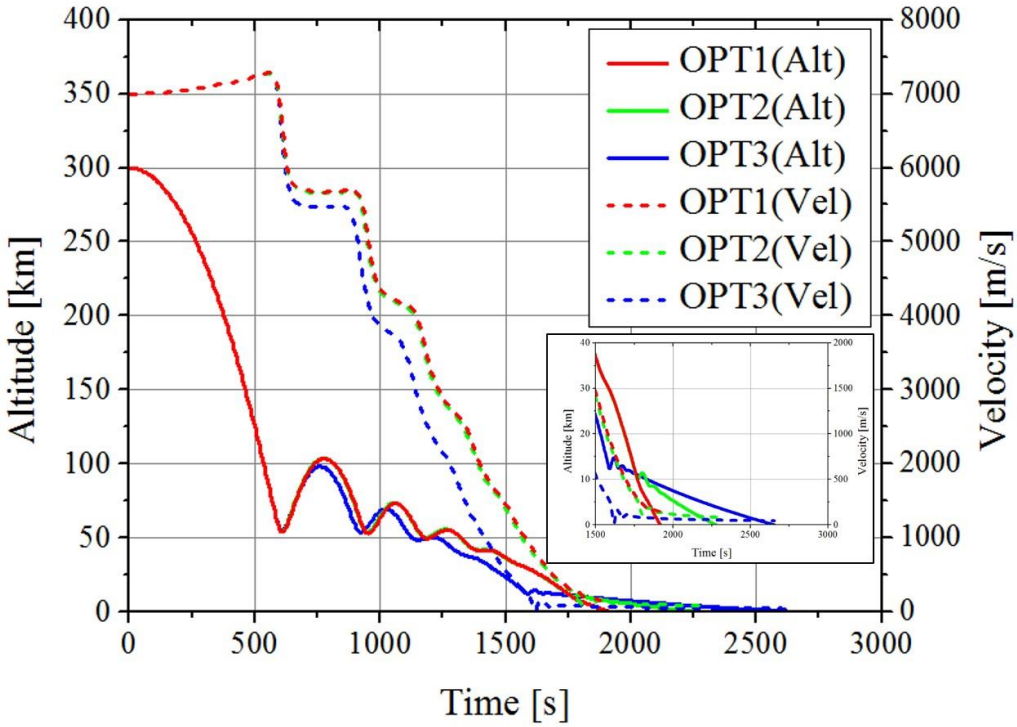

Figure 12: Altitude and velocity of OPT1-3 with time.

5 Conclusion

In this study, reusable unmanned space vehicles that start falling from a low-earth orbit (LEO) and land on the ground are designed conceptually with multi objective functions. To do so, an MDO was constructed consisting of vehicle geometry definition, weight analysis, propulsion analysis,

aerothermodynamic analysis, trajectory analysis, and a multi-objective genetic algorithm (MOGA). There were three objectives: minimize weight, maximize the highest C_L in the supersonic range and minimize landing speed. The maximum heat flux and maximum dynamic pressure must be below 4MW/m2 and 50kPa as constraints, respectively, and longitudinal stability should be maintained. The extreme solutions were selected in the Pareto solution, and the geometry and performance were compared according to the objective functions. All objective functions are in trade-off relationships with each other. Furthermore, conceptually designed geometries increased the maximum C_L by widening the area directly receiving the flow. The overall weight of the lightest vehicle was reduced by reducing the size of the wings. In the supersonic region, the vehicle with the largest maximum C_L had a closer angle between the flow and the lower surface of the wing than the angle that resulted in the highest C_L. The vehicle with the lowest landing speed achieved sufficient deceleration with the largest wing size.

Acknowledgement

This work is supported by a grant from the National Research Foundation of Korea (NRF-2017M1A3A3A02016269). Images in this paper were created using FieldView, as provided by Intelligent Light through its University Partner Program.

References

[1] W. E. Hammord. *Design methodologies for space transportation system.* AIAA, 2001.
[2] R. Lawrence and D. Robert. Multidisciplinary conceptual design optimization of space transportation system. J. Aircraft, 36:218-226, 1999.
[3] T. Tsuchiya and T. Mori. Optimal conceptual design of two-stage reusable rocket vehicles including trajectory optimization. J. Spacecraft and Rocket, 41:770-778, 2004.
[4] T. Tsuchiya, Y. Takenaka and H. Taguchi. Multidisciplinary design optimization for hypersonic experimental vehicle. AIAA J., 45:1655-1662, 2007.
[5] N. Yokoyama, S. Shinji, T. Tsuchiya, H. Taguchi and T. Kanda. Multidisciplinary design optimization for space plane considering rigid body characteristics. J. Spacecraft and Rocket, 44:121-131, 2007.
[6] A. Hashimoto, S. Jeong and S. Obayashi. Aerodynamic optimization of near-future high-wing aircraft. Trans. JSASS, 58:73-82, 2015.
[7] G. J. Harloff and B. M. Berkowiz. HASA-hypersonic aerospace sizing analysis for the preliminary design of aerospace vehicles. NASA CR-182226, 1988.
[8] R. R. Rohrschneider. Development of a mass estimating relationship database for launch vehicle conceptual design. Georgia Institute of Technology, 2002.
[9] Y. Nakata, S. Taura, T. Nakayama and N. Nakagawa. Advanced integrated modular avionics. J. JSASS, 52:2-9, 2004.
[10] C. George. X-37 Demonstrator to test future launch technologies in orbit and reentry environments. NASA FS-2003-05-65-MSFC, 2003.
[11] D. J. Anderson. *Modern compressible flow.* Mc. Graw Hill, 2004.
[12] R. Fink. USAF stability and control DATCOM. AFWAL-TR-83-3048.
[13] D. J. Gamble, R. D. Cooke, M. J. Underwood, W. H. Stone and C. D. Schlosser. The development and application of aerodynamic uncertainties and flight test verification for the space shuttle orbiter. NACA CP-2342, Part 1, N82-16910, 1985.
[14] X. Liu, Z. Shen and P. Lu. Entry trajectory optimization by second-order cone programming. J. Guidance, Control, and Dynamics, 39:227-241, 2016.